

# Leakage Current Induced by Energetic Disorder in Organic Bulk Heterojunction Solar Cells: Comprehending the Ultrahigh Loss of Open-Circuit Voltage at Low Temperatures

Wenchao Yang,<sup>1</sup> Yongsong Luo,<sup>1</sup> Pengfei Guo,<sup>1</sup> Haibin Sun,<sup>1</sup> and Yao Yao<sup>2,\*</sup>

<sup>1</sup>*School of Physics and Electronic Engineering, Xinyang Normal University, Xinyang 464000, China*

<sup>2</sup>*Department of Physics, South China University of Technology, Guangzhou 510640, China*

(Received 14 November 2016; revised manuscript received 13 March 2017; published 19 April 2017)

The open-circuit voltage ( $V_{oc}$ ) of organic solar cells generally approaches its maximum obtainable values as the temperature decreases. However, recent experiments have revealed that the  $V_{oc}$  may suffer from an ultrahigh loss at low temperatures. In order to verify this explanation and investigate the impacts of energetic disorder on the temperature-dependent behaviors of the  $V_{oc}$  in general, we calculate the  $V_{oc} - T$  plots with the drift-diffusion method under various device working parameters. With the disorder being incorporated into the device model by considering the disorder-suppressed (temperature-dependent) charge-carrier mobilities, it is found that the ultrahigh  $V_{oc}$  losses cannot be reproduced under the Onsager-Braun-type charge generation rate. With the charge generation rate being constant or weakly dependent on temperature, for nonselective contacts, the  $V_{oc}$  reduces drastically at low temperatures, while for selective contacts, the  $V_{oc}$  increases monotonically with decreasing temperature. With higher carrier mobilities or smaller device thicknesses, the ultrahigh loss occurs at lower temperatures. The mechanism is that, since the disorder-suppressed charge mobilities give rise to both low charge-extraction efficiency and small bimolecular recombination rate, plenty of charge carriers can be extracted from the wrong electrode and can form a large leakage current, which counteracts the majority-carrier current and reduces the  $V_{oc}$  at low temperatures. Our results thus highlight the essential role of charge-carrier kinetics, except for the charge-filling effect, on dominating the disorder-induced  $V_{oc}$  losses.

DOI: 10.1103/PhysRevApplied.7.044017

## I. INTRODUCTION

For the state-of-the-art organic bulk heterojunction solar cells, the power conversion efficiency has exceeded 10% through decades of efforts on the optimization of device structures and internal morphology [1]. Nevertheless, they are far from commercial applications due to the ubiquitously low open-circuit voltages ( $V_{oc}$ ) of no more than 1 V, which implies a remarkable loss when comparing the  $eV_{oc}$  with the effective band gap, namely, the energy offset between the lowest unoccupied molecular orbital (LUMO) of the acceptor and the highest unoccupied molecular orbital (HOMO) of the donor [2]. In order to reveal the origin of the  $V_{oc}$  loss and find a means to minimize it, people have investigated extensively the relationships between the  $V_{oc}$  and various types of electronic properties or processes, such as the charge-transfer (CT) state energy [3–8], the charge recombination dynamics [9,10], the charge-carrier densities [11], the energetic disorder [12–15], the light intensity [16,17], the internal molecular morphology [18], the metal-organic contact properties [10,19–21], and so on. The results suggest that the  $V_{oc}$  is intricately correlated with all of these factors, and an elaborate theoretical formulation of the  $V_{oc}$  is highly desirable [22].

There are generally two fundamental principles from which the basic expressions of the  $V_{oc}$  and the corresponding loss can be deduced. First, electrically, the  $V_{oc}$  is basically determined as the minimum electron-hole quasi-Fermi-level splitting within the active layer under the open-circuit condition [19], namely, the nonequilibrium steady state in which the charge generation rate  $G$  is exactly equal to the charge recombination rate  $R$  [12]. Second, optically, a detailed balance is established between the reversal processes of optical absorption and electroluminescence (radiative recombination) in a working solar cell [4,5,23]. The  $V_{oc}$  formula based on the two principles gives rise to the same behavior of the  $V_{oc}$  versus the variation of temperature; that is, the  $V_{oc}$  merely increases linearly with the decreasing temperature until saturating to its maximum value at the low-temperature limit. This  $V_{oc} - T$  relation has been experimentally demonstrated very well [24,25], and it is very useful for characterizing the device properties. For instance, by measuring the slope of the  $V_{oc} - T$  plots, people can determine the diode ideality factors under illuminated conditions. The only distinction between the two formulations lies in the fact that they predict different maximum achievable values of the  $V_{oc}$ . Based on the first principle, the maximum  $eV_{oc}$  should be the effective band gap  $E_g$  [11,24], while, following the second one, it is the CT-state energy  $E_{CT}$  [3,7,8,25]. When taking the energetic disorder effect of the LUMO or HOMO levels or the dense

\*yaoyao2016@scut.edu.cn

CT-state manifolds ubiquitous at the organic donor-acceptor interface into account, the density of states (DOS) therein is greatly broadened and extended to the band gap, leaving a significant DOS tail in the gap. The  $V_{oc}$  expression should then be corrected due to the relaxation of charge carriers to the tail states or the CT excitons to the low-lying vibronic states [26,27]. In the former case, with the Gaussian-disorder model, the total  $V_{oc}$  expression can be written as

$$eV_{oc} = E_g - \frac{\sigma_n^2 + \sigma_p^2}{2kT} - kT \ln\left(\frac{N_c N_v}{np}\right), \quad (1)$$

where  $\sigma_n$  ( $\sigma_p$ ) is the width of the LUMO (HOMO) DOS, and the other notations follow the common definitions [12–14]. In the latter case, the expression is changed only by replacing the second term on the right-hand side of Eq. (1) with  $\sigma_{CT}^2/2kT$ , in which  $\sigma_{CT}$  is the DOS width of the CT-state manifold [6,28]. Thus, with disorder being incorporated, the  $V_{oc} - T$  relations deduced from the two principles remaining follow the same behavior, even though the respective physical meanings of the disorder may be different. At around room temperature (RT), the  $V_{oc} - T$  relation is still dominated by linearly increasing behavior as the temperature reduces. In the low-temperature regime, however, the correction term which is inversely proportional to the temperature becomes very significant. Except for reducing the maximum achievable  $V_{oc}$ , it makes the  $V_{oc}$  increase gradually and saturate slower with a decreasing temperature.

Recently, Gao *et al.* observed an unusual phenomenon in which certain types of polymer-fullerene-blended solar cells, as the temperature decreases at around RT, the  $V_{oc}$  initially increases linearly as expected, but it begins to decrease at a particular low temperature [29]. To our knowledge, it is the first observation of the nonmonotonic behavior of the  $V_{oc}$  versus the  $T$  relation, and its underlying mechanism needs to be elucidated. Gao *et al.* attributed it to the simultaneous decrease of the photogenerated charge-carrier density because of the diminishment of entropy-driven charge-separation process at low temperatures [30,31], which could reduce the  $V_{oc}$ , according to the third term on the right-hand side of Eq. (1). However, this argument has not been verified quantitatively through device-simulation works. On the other hand, it can be expected that, at low temperatures, the energetic disorder may suppress the linearly increasing behavior of the  $V_{oc}$ , as stated above. Unfortunately, this effect cannot explain the phenomenon either. With realistic energetic-disorder parameters substituted into Eq. (1), the calculated  $V_{oc} - T$  relation still gives rise to monotonically increasing behavior with a decreasing temperature [13].

In this work, we endeavor to find the origin of this anomalous reduction of the  $V_{oc}$  through the calculations of the current-density–voltage ( $J$ - $V$ ) curves and the  $V_{oc} - T$

relations for various device parameters and working conditions. Specifically, we incorporate the disorder-suppressed charge-carrier mobility obtained through the kinetic Monte Carlo simulations for organic solid into the device model, which is found to be a key factor for inducing ultrahigh  $V_{oc}$  loss. The results are beneficial for a comprehensive understanding of the underlying mechanisms through which the disorder effect may damage the performance of organic bulk-heterojunction solar cells, and they also provide an alternative perspective for investigating the origin of the  $V_{oc}$  loss from the steady-state charge-carrier dynamics. This paper is organized as follows: In Sec. II, the drift-diffusion simulation method and the energetic disorder model are introduced. In Sec. III, we systematically investigate the conditions at which the ultrahigh loss can be reproduced, the impacts of material and device parameters on the loss, and its origin. The conclusions are then presented in Sec. IV.

## II. DEVICE-MODEL METHOD

The device-model (drift-diffusion) method is commonly employed for simulating the macroscopic device operating properties. In this model, the photoactive layer is basically considered a homogeneous medium. Then the time evolution of the photogenerated CT states and the charge carriers are described by the following one-dimensional continuity equations:

$$\frac{\partial X}{\partial t} = D_X \frac{\partial^2}{\partial x^2} - k_d X - \frac{X}{\tau} + G, \quad (2)$$

$$\frac{\partial p}{\partial t} = -\frac{1}{e} \frac{\partial J_p}{\partial x} + k_d X - R(x), \quad (3)$$

$$\frac{\partial n}{\partial t} = \frac{1}{e} \frac{\partial J_n}{\partial x} + k_d X - R(x). \quad (4)$$

$X$ ,  $p$ , and  $n$  denote the densities of the CT states, the holes, and the electrons, respectively. On the right-hand side of Eq. (2), the first term stands for the CT states' diffusion (with  $D_X$  being the diffusivity), the second one for the CT states' dissociation and charge formation (with  $k_d$  being the dissociation rate), the third one for the radiative and nonradiative decay of the CT states to the ground state (with  $\tau$  being the lifetime), and the fourth term for the photogeneration of the CT states (with  $G$  representing the generation rate). The hole (electron) current density in Eq. (3) [Eq. (4)] is of the common drift-diffusion form in which the Einstein's relation has been assumed:

$$J_{p(n)}(x) = e\mu_{p(n)} \left( p(n)E \mp \frac{kT}{e} \frac{\partial p(n)}{\partial x} \right). \quad (5)$$

The spatiotemporal evolution of the internal electric field  $E$  is governed by Poisson's equation, which reads

$$\frac{\partial E}{\partial x} = \frac{e}{\epsilon_0 \epsilon} (p - n). \quad (6)$$

The boundary conditions of the equations are imposed through properly giving the electron-hole current density at the two metal-organic contacts. For instance, the hole current density on the anode side and the electron current on the cathode side are

$$J_p(0) = qS_p[p(0) - p_0], \quad (7)$$

$$J_n(L) = -qS_n[n(L) - n_0], \quad (8)$$

in which  $S_{p(n)}$  is the surface recombination velocity for holes (electrodes) and is determined to be  $AT^2/N_{v(c)}$ , with  $A$  being the Richardson's constant from the detailed-balance principle [32] and  $p_0$  ( $n_0$ ) the equilibrium hole density therein. For the nonselective contacts, the hole (electron) current density at the cathode (anode)  $J_p(L)$  [ $J_n(0)$ ] can be written in a similar form as Eq. (7). For the selective contacts, the surface recombination velocity for the minority carriers is fixed to zero and the wrong electrode charge extraction is completely quenched, i.e.,

$$J_n(0) = J_p(L) = 0. \quad (9)$$

With the imposed boundary conditions, Eqs. (2)–(4) and (6) can be solved numerically to investigate many types of macroscopic quantities for a working device. The details for device-model implementation are elaborated on in numerous locations in the literature and thus are omitted here [32–34]. In our simulation, the Onsager-Braun theory is initially incorporated into the model to account for the temperature variation of the CT-state dissociation (or charge generation) rate, which can be written as [33,35]

$$k_d = \frac{3\gamma}{4\pi a^3} \exp\left(-\frac{E_b}{kT}\right) \left(1 + b + \frac{b^2}{3} + \frac{b^3}{18}\right), \quad (10)$$

where the parameter is

$$b = \frac{e^3 F}{8\pi \epsilon_0 \epsilon k^2 T^2}, \quad (11)$$

and

$$\gamma = \frac{e(\mu_n + \mu_p)}{\epsilon_0 \epsilon} \quad (12)$$

is the Langevin recombination coefficient.  $E_b = e^2/4\pi\epsilon_0\epsilon a$  is the CT-state binding energy, with  $a$  representing the CT-state radius. The other notations follow the common definitions. For the recombination rate  $R$ , the bimolecular recombination (BR) is assumed to be the dominant recombination mechanism, namely,

$$R = \gamma(np - n_i^2). \quad (13)$$

For polymer-fullerene solar cells,  $R$  is generally reduced by orders of magnitude compared to the Langevin-type BR rate [36]. In this case, the right-hand side of Eq. (13) should be multiplied by a BR reduction factor  $\zeta$ , and its value may depend on the extent of phase separation in the donor-acceptor blend [37], the impact of the image-charge effect, and so on [38]. The reduced BR effect on the  $V_{oc} - T$  relations is also investigated in our simulations.

When the effects of the intrinsic energetic disorder are to be investigated, instead of analyzing the effective reduction of the quasi-Fermi-level splitting due to the charge filling in the tail states [13,14], we incorporate it into the device model by considering its influence on the charge-transport properties. With the presence of the disorder, the charge carriers undergo the phonon-assisted hopping motion due to the induced charge-localization effect. By employing semiclassical numerical methods like the kinetic Monte Carlo simulation, the nonequilibrium steady-state charge mobilities  $\mu$  are calculated many times for the Gaussian-disorder model, and they are found to be of the following temperature dependence[39–43]:

$$\mu = \mu_\infty \exp\left[-\left(c \frac{\sigma}{kT}\right)^2\right], \quad (14)$$

where  $\mu_\infty$  is the high-temperature limit of the mobility,  $\sigma$  is the Gaussian-disorder width, and the coefficient  $c$  is set at  $2/3$  [1]. According to Eq. (14), the mobility is strongly suppressed by the energetic disorder under low temperatures. In addition, the same calculations also reveal that the energetic disorder can make the charge mobility become dependent on the charge density and the electric field, but these two dependencies become significant only when the carrier density and the electric-field strength are sufficiently high, as they are in organic field-effect transistors. However, in organic solar cells, these effects are negligible, and they are excluded from our model for the sake of simplicity. It should be noted that, if the temperature-dependent mobility [Eq. (14)] is involved when calculating the steady-state quantities, with decreasing temperature, the evolution time required for the device to reach the steady state becomes longer and thus needs to be enhanced accordingly. The simulation parameters are listed in Table I, except where otherwise noted.

TABLE I. The parameters used in the device-model simulation.

Parameter	Symbol	Value
Effective band gap	$E_g$	1.3 eV
Injection barriers	$\phi_n, \phi_p$	0.2 eV
Relative permittivity	$\epsilon$	3.5
Active-layer thickness	$L$	200 nm
Density of states	$N_C, N_V$	$10^{21} \text{ cm}^{-3}$
High- $T$ mobility	$\mu_\infty$	$0.1 \text{ cm}^2/\text{V s}$
CT generation rate	$G$	$3 \times 10^{21} \text{ cm}^{-3} \text{ s}^{-1}$
CT-state lifetime	$\tau$	100 ns
CT-state radius	$a$	2 nm

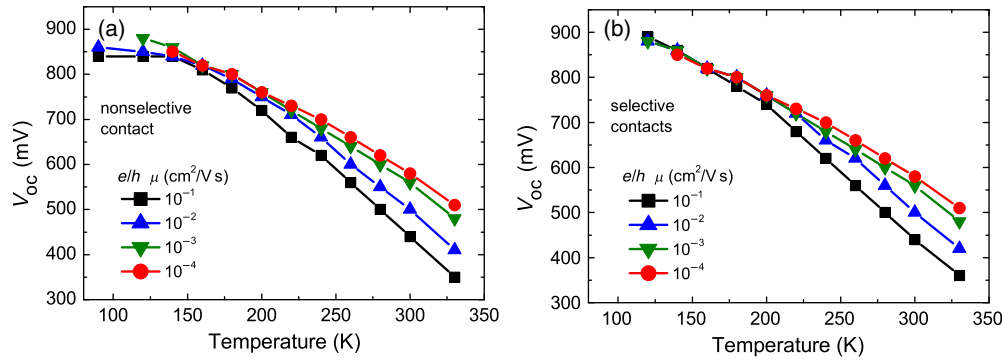


FIG. 1. (a) The  $V_{oc} - T$  plots calculated under a set of balanced electron and hole mobilities with nonselective contacts. (b) The  $V_{oc} - T$  plots calculated under the same condition, but with selective contacts being assumed. The Onsager-Braun-type CT-state dissociation rate  $k_d$  is incorporated into the calculations of both of the plots.

### III. RESULTS AND DISCUSSION

#### A. Conditions of the ultrahigh loss

First of all, we attempt to verify the hypothesis that the decreased photogenerated charge-carrier density causes the reduction of the  $V_{oc}$  at low temperatures. Meanwhile, the influence of the metal-organic interfacial properties on the  $V_{oc}$  are also examined by assuming different boundary conditions in the device model. With constant and balanced electron-hole mobilities being substituted into the model, we calculate the  $J-V$  curves for a set of temperatures ranging from 320 K down to ones at which the photogenerated charge carriers are very limited and the photocurrent decreases approximately to zero (for instance, 100 K). From the  $J-V$  curves, the  $V_{oc}$ 's corresponding to each temperature can be extracted. In Fig. 1, the  $V_{oc} - T$  curves with nonselective and selective contacts for charge-carrier extraction are shown, respectively. It is found that, as temperature decreases from above RT, the linearly increasing behavior of the  $V_{oc}$  is clearly reproduced for both types of contacts. With nonselective contact, when the temperature is reduced to 150 K, the  $V_{oc}$ 's gradually saturate to below 900 mV, which is the maximum achievable  $V_{oc}$  given by the band gap subtracting the energy offset due to the electron- and hole-injection barriers. For higher carrier mobilities such as  $0.1 \text{ cm}^2/\text{Vs}$ , the calculated  $V_{oc}$  is relatively lower and saturates earlier with the decreasing temperature since high mobility may bring about a large bimolecular recombination rate [see Eq. (12)] and severe surface losses due to the extraction of charge carriers from

the wrong electrode. With selective contact, the  $V_{oc} - T$  plots for different mobilities converge below 180 K. They exhibit no obvious saturation behavior, but they finally approach 900 mV at low temperatures because of the absence of the surface losses. Under these conditions, no  $V_{oc}$  reduction is observed, which suggests that it is not sufficient to explain this phenomenon solely by the reduction of charge-carrier density with a decreasing temperature due to the entropy effect or according to the Onsager-Braun theory, and, for the constant-mobility cases, the metal-organic contact properties have little influence on the behaviors of the  $V_{oc}$ . In the following, except where stated explicitly to the contrary, all of the simulations are done under nonselective contacts.

Next, we examine the influence of the energetic disorder on the  $V_{oc} - T$  relations. Incorporating Eq. (14) and the Onsager-Braun charge generation rate of Eq. (10) into the device model, the  $J-V$  curves for different temperatures are calculated and presented in Fig. 2(a), in which the Gaussian disorder  $\sigma$  is set to 80 meV. It is observed that, as the temperature decreases, the reduction of the short-circuit current density  $J_{sc}$  becomes more and more drastic because of the quick reductions of both the charge-carrier generation rate and the mobilities, while the  $V_{oc}$  increases more and more slowly in the low-temperature regime but exhibits no reduction behavior. In Fig. 2(b), the calculated  $V_{oc} - T$  plots for a wide range of Gaussian-disorder parameter  $\sigma$ 's are shown. For a small disorder such as  $\sigma = 50$  meV, the linearly increasing behavior is still retained at a relatively large temperature range before the final saturation. For a

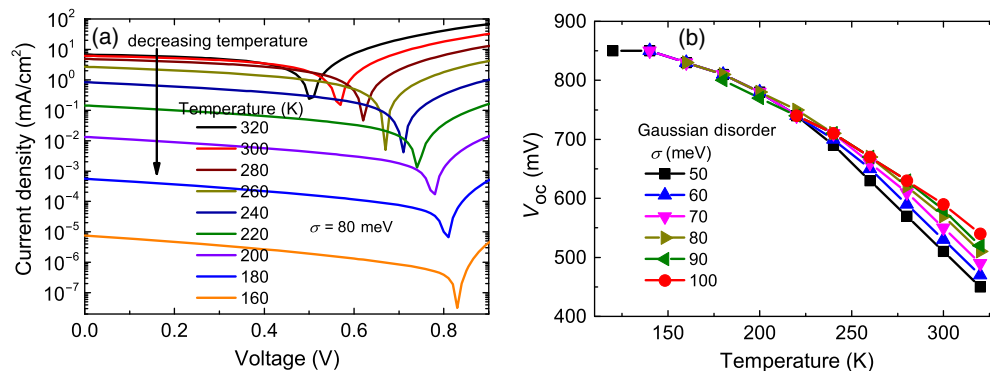


FIG. 2. (a) The  $J-V$  curves calculated at different temperatures with disorder-suppressed mobilities, in which the energetic disorder  $\sigma = 80$  meV. (b) The calculated  $V_{oc} - T$  plots with the disorder-suppressed carrier mobilities. The Onsager-Braun-type CT-state dissociation rate  $k_d$  is incorporated into the calculations.

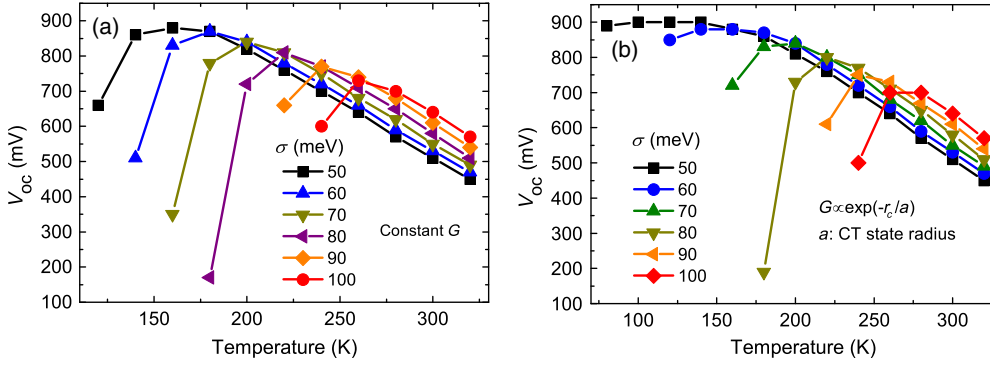


FIG. 3. (a) The calculated  $V_{oc} - T$  plots for fully constant charge generation rate and disorder-suppressed mobilities, with different Gaussian-disorder values being assumed. (b) The calculated  $V_{oc} - T$  plots under the same conditions as (a) except that a temperature-dependent charge generation rate which is proportional to  $\exp(-r_c/a)$  (with  $r_c$  being the Coulomb capture radius) is assumed.

high disorder like  $\sigma = 100$  meV, although the  $V_{oc}$  at RT is slightly higher, it increases rather slowly (see the slope change of the  $V_{oc} - T$  plots for different  $\sigma$ 's at the high-temperature regime) and quickly deviates from linearly increasing behavior with decreasing temperature. In the low-temperature regime, the  $V_{oc} - T$  plot with  $\sigma = 100$  meV tends to saturate to a small value of less than 800 mV. Nevertheless, even for such a high energetic disorder, the corresponding  $V_{oc} - T$  plot still increases monotonically with decreasing temperature. Therefore, the combined effect of the strongly temperature-dependent charge generation rate and the disorder-suppressed mobilities does not lead to the reduction of the  $V_{oc}$  at low temperatures.

We consider the sole effect of disorder-suppressed mobilities on the  $V_{oc}$  loss. By retaining Eq. (14) for the disorder-suppressed mobilities but employing a fully constant charge-carrier generation rate  $G$  in the simulation, the  $V_{oc} - T$  plots are calculated and shown in Fig. 3(a). In the RT regime, the linearly increasing behavior of the  $V_{oc}$ 's remains unchanged for different disorder  $\sigma$ 's. The higher the disorder, the larger the  $V_{oc}$  because the disorder-suppressed mobilities give rise to a small bimolecular recombination coefficient  $\gamma$  and thus small bulk recombination losses. More importantly, the reduction of the  $V_{oc}$  indeed shows up for each disorder parameter  $\sigma$  when the temperature decreases below a critical value, where the  $V_{oc}$  reaches its maximum value and an ultrahigh loss emerges. With a small  $\sigma$  of 50 meV, this critical temperature is around 160 K. As the disorder increases, the critical temperature increases monotonically. When  $\sigma = 100$  meV, the critical temperature is as high as 260 K and the maximum  $V_{oc}$  is only 750 mV. Compared with the experimentally measured  $V_{oc} - T$  plots by Gao *et al.*, the simulated decreasing behavior is much more drastic, which could be attributed to the strongly temperature-dependent mobilities employed in our simulations, but in real systems the temperature variation of mobilities could be much milder than that described by Eq. (14).

The reproduction of the experimentally observed  $V_{oc}$  reduction behavior under the constant charge generation rate

$G$  in Fig. 3(a) also suggests that the Onsager-Braun theory is not applicable in this case, which greatly overestimates the impact of temperature on the CT-state dissociation processes. Actually, the failure of the Onsager-Braun theory is consistent with the finding that a high percentage of charge carriers is generated through the ultrafast interfacial charge-transfer process due to quantum coherence, which is expected to be more prominent at low temperatures, rather than the thermal-assisted dissociation of the relaxed CT states [44–46]. On the other hand, it is also unrealistic to assume that the charge-carrier generation rate is absolutely temperature independent. Therefore, we substitute  $\gamma$  [Eq. (12)] that is free of disorder into Eq. (10) and let the temperature dependence of the dissociation rate  $k_d$  be dominated by the Coulomb capture radius  $r_c$ , defined as  $r_c = e^2/4\pi\epsilon_0\epsilon kT$  and appearing only in the factor of  $\exp(-r_c/a) = \exp(-E_b/kT)$ . With such a relatively weakly temperature-dependent  $k_d$ , the  $V_{oc} - T$  plots for different disorder  $\sigma$ 's are calculated and shown in Fig. 3(b). It can be observed that the main features of these plots remain the same as those shown in Fig. 3(a), except that, for small  $\sigma$ 's, the decreasing behavior of the  $V_{oc}$  becomes moderate in the low-temperature regime, which more closely resembles the experimentally measured  $V_{oc} - T$  plots. Therefore, we can conclude that it is the disorder-suppressed mobilities that primarily induce the ultrahigh  $V_{oc}$  loss at low temperatures.

## B. Impacts of charge recombination and extraction

To gain deeper insight into the impact of BR on the  $V_{oc}$  loss in general, we calculate the  $V_{oc} - T$  relations with a fixed BR reduction factor  $\zeta$  being taking into account for  $R$ , as shown in Fig. 4(a). It is apparent that the reduction behavior of the  $V_{oc}$  is also reproduced for all of the plots. In the RT regime, with a smaller  $\zeta$ , the BR rate is reduced and the corresponding  $V_{oc}$  is higher because the photogenerated charge carriers are less likely to be lost through the BR pathway, which has been demonstrated in our previous work [21]. Meanwhile, in the low-temperature regime, the smaller  $\zeta$  gives rise to a higher critical temperature below which a reduction of the  $V_{oc}$  takes place, implying that the reduced BR may play an essential role in inducing the

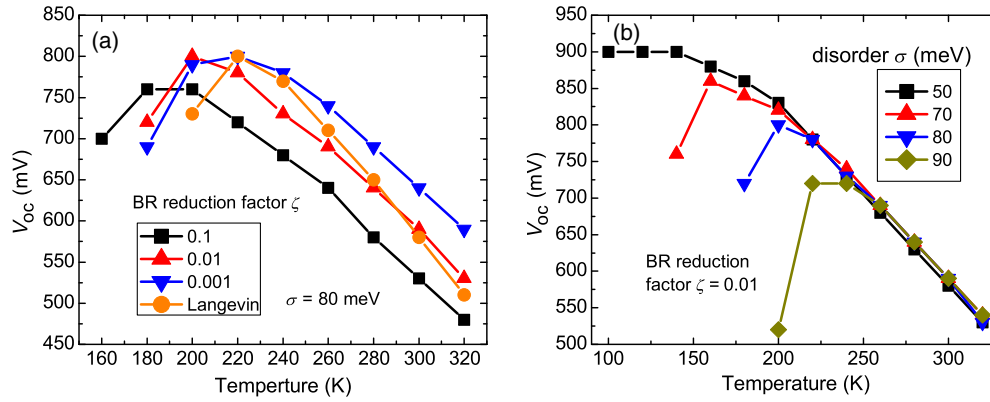


FIG. 4. (a) The calculated  $V_{oc} - T$  plots for the fixed BR reduction factor  $\zeta$ 's differing by an order of magnitude and where  $\sigma = 80$  meV. By comparison, the plot for the temperature-dependent Langevin-type BR rate is also included. (b) The calculated  $V_{oc} - T$  plots for different energetic disorder  $\sigma$ 's with the same fixed  $\zeta$  of 0.01.

ultrahigh  $V_{oc}$  loss effect. There also exists an effective  $\zeta$  inherent in the disorder-suppressed Langevin-type BR rate, namely, the exponential factor contained in the disorder-suppressed mobilities [see Eq. (14)]. It is initially close to unity at RT but decreases very rapidly to small values as the temperature decreases, so that the corresponding  $V_{oc}$  exhibits both a faster linearly increasing behavior in the RT regime and a more drastic decreasing one at a higher critical temperature than those corresponding to fixed  $\zeta$ 's. This temperature-dependent BR reduction effect has been experimentally verified through the photogenerated charge extraction by linearly increasing voltage and the pump-probe technique, respectively [47,48]. The  $\zeta$  could be an Arrhenius-type one with the activation energy resulting from the barriers for polaron hopping transport and having the same magnitude as the disorder  $\sigma$ 's employed here [38], or similar to the form employed by us [47]. In Fig. 4(b), the calculated  $V_{oc} - T$  relations for a set of  $\sigma$ 's with the same  $\zeta$  of 0.01 are presented. Compared to Fig. 3(b), the  $V_{oc}$ 's corresponding to different  $\sigma$ 's cannot be distinguished from each other in the RT regime, which is unlike the experimentally obtained plots. Thus, it is reasonable to employ the temperature-dependent BR rate when the disorder-related effects are examined in device modeling.

Furthermore, we investigate how the  $V_{oc} - T$  relationship may be influenced by the electron-hole mobilities and the thickness of the active layer. The high-temperature limit of mobilities  $\mu_{\infty}$  can vary among different material systems

or device-preparation conditions. At a specific temperature, the increased  $\mu_{\infty}$  implies increased mobility, which subsequently leads to a high BR rate and a high charge-extraction efficiency. We calculate the  $V_{oc} - T$  relations with the disorder  $\sigma = 80$  meV for a set of typical values of  $\mu_{\infty}$ , as shown in Fig. 5(a). It is observed that, for higher  $\mu_{\infty}$ 's such as that of  $10 \text{ cm}^2/\text{V s}$ , the linearly increasing  $V_{oc} - T$  relationship can be extended to relatively low temperatures so that the higher maximum obtainable  $V_{oc}$ 's can be reached in this case, and the critical temperature declines accordingly. As for the  $V_{oc}$  in the RT regime, it follows the tendency of decreasing with an increased  $\mu_{\infty}$  due to the induced high BR losses.

The calculated  $V_{oc} - T$  relations for the varied thickness  $L$  are shown in Fig. 5(b). Around the RT, the  $V_{oc}$ 's are just slightly higher for devices of thinner active layers. The major differences emerge in the low-temperature regime, where a thinner device with an  $L$  smaller than 100 nm can maintain a relatively high  $V_{oc}$  which decreases slowly. For thick devices, however, the reduction of the  $V_{oc}$ 's are more drastic. With an increased  $L$ , the internal electric field  $E$  becomes small since  $E = V_{\text{eff}}/L$ , where the effective potential  $V_{\text{eff}}$  is equal to the difference between the applied bias voltage  $V_a$  and the built-in potential  $V_{\text{bi}}$ , and the sweeping (extraction) time for free charge carriers  $t_{\text{ex}} = L^2/2V_{\text{eff}}\mu$  increases accordingly, which causes the charge-extraction efficiency to be reduced. Combined with the mobility-dependent results shown in Fig. 5(a), they suggest that the reduced

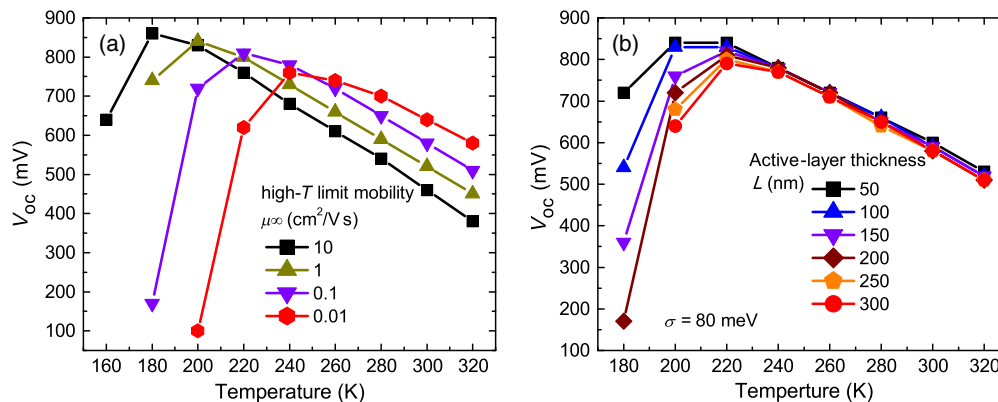


FIG. 5. (a) The calculated  $V_{oc} - T$  plots for different high-temperature limits of mobilities  $\mu_{\infty}$ . (b) The calculated  $V_{oc} - T$  plots for different active-layer thicknesses  $L$ . The disorder  $\sigma$  is set to 80 meV in both (a) and (b). Other parameters and conditions in the simulations are kept the same as those in Fig. 3.

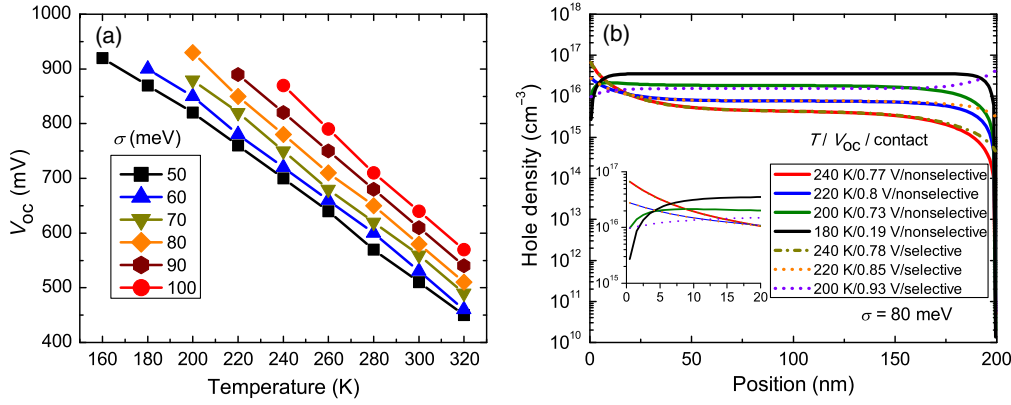


FIG. 6. (a) The calculated  $V_{oc} - T$  plots for different Gaussian-disorder  $\sigma$ 's under the selective contacts for both anode-organic and organic-cathode interfaces. Other parameters and conditions in the simulations are kept the same as those in Fig. 3. (b) The calculated hole density profiles under the open-circuit conditions for different temperatures and contact types. To show the anode-organic interfacial hole distribution clearly, the density profiles in the region of 0–20 nm are magnified and plotted in the inset.

free charge extraction may be one of the underlying reasons for the ultrahigh losses of the  $V_{oc}$ . Other device working conditions or parameters such as the light intensity are varied for further simulations, but they are found to have only slight impacts on the temperature-dependent behavior of the  $V_{oc}$  and, therefore, are not shown here.

### C. Origin of the ultrahigh loss

In Fig. 6(a), we present the calculated  $V_{oc} - T$  plots for a different disorder  $\sigma$  under selective contacts while keeping the other parameters the same as those in Fig. 3(b). It can be observed that the behavior of the  $V_{oc}$ 's is significantly changed, especially for those with large  $\sigma$ 's. They increase only monotonically with an approximately constant slope as the temperature decreases, in contrast to the abrupt reduction behavior under nonselective contacts. Moreover, the electron- and hole-injection barriers no longer impose a restriction on the  $V_{oc}$ , and the latter can exceed 900 mV at low temperatures. To reveal the underlying mechanism of the contact-induced  $V_{oc}$  behavior, we calculate the hole density profiles under the open-circuit conditions for both selective (dashed lines) and nonselective (solid lines) contacts, with  $\sigma = 80$  meV, as shown in Fig. 6(b). Comparing the two curves corresponding to the different contact types at the same temperature, it is apparent that they precisely overlap in the bulk region of the device, but they diverge from each other at the vicinity of the two contacts. This divergence between the nonselective and selective curves becomes more and more significant with decreasing temperatures. For instance, at temperatures of 240 and 220 K, the overlapped region on the curves extends to the anode where the hole density is much higher than those in the bulk. Thus, the electrons flowing to the anode, which consists of one component of the wrong electrode currents, are effectively annihilated through the intensive BR with the accumulated holes at the interface, making the nonselective contacts essentially selective at relatively high

temperatures. At low temperatures, on the other hand, although the bulk hole density is enhanced as a result of the rapid decrease of the BR coefficient  $\gamma$ , the interfacial hole density, which can be approximated by the equilibrium density  $p_0 = N_v \exp(-\phi/kT)$  (with  $\phi$  being the injection barrier) due to the high surface recombination velocity  $S_p$ , is greatly diminished; it can even be lower than that in the bulk, such as those observed in the nonselective curves of  $T = 200$  and 180 K. The consequence is that, under the nonselective contacts, the recombination is weak without sufficient holes and a huge number of electrons in the bulk may flow into the anode unblocked, which brings about significant charge-carrier losses and an ultrahigh  $V_{oc}$  loss.

This loss mechanism can be manifested by the calculated curves of the electron current density at the anode side  $J_n^{an}$  versus voltages for various temperatures, as shown in Fig. 7(a). The complete  $J-V$  curves are also presented in Fig. 7(b) for reference. At temperatures near RT, owing to the aforementioned efficient electron blocking effect induced by the high hole density near the contact, the  $J_n^{an}$  is small and does not increase very much with an increasing bias voltage. At low temperatures (see the curves of 200 or 180 K), however, the blocking effect vanishes gradually and the  $J_n^{an}$  increases very rapidly. The reason is that plenty of free electrons (holes) are accumulated in the bulk due to the greatly reduced BR rate at low temperatures, and without blocking layers, these electrons (holes) can be easily extracted to the anode (cathode) with an external electric field, forming a large leakage current. The  $J_n^{an}$  is just the leakage current combined with the dark injected electron current. In other words, the free electrons are lost mostly through the surface recombination rather than the diminished BR in the bulk. On the other hand, the hole current  $J_p^{an}$  is very small, as a result of the disorder-suppressed low mobility (or the low extraction efficiency). The leakage current counteracts the hole current and surpasses it under a small bias voltage, making the direction

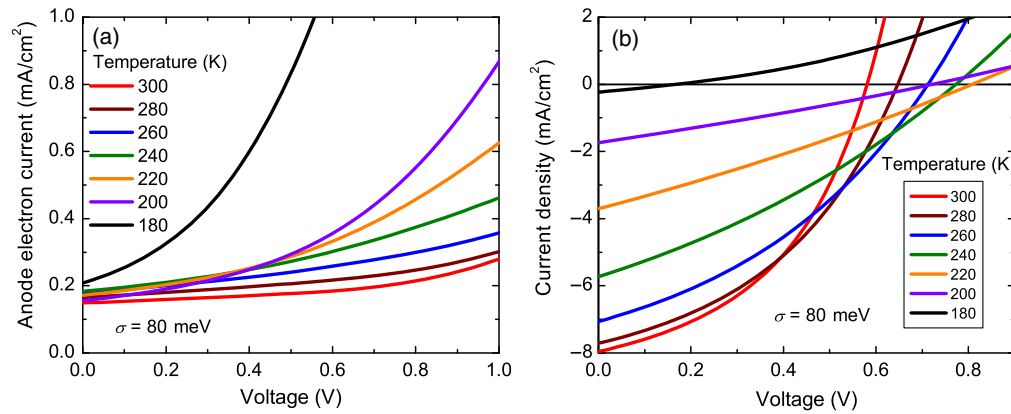


FIG. 7. (a) The  $J_n^{\text{an}}-V$  curves under nonselective contacts for different temperatures, where  $J_n^{\text{an}}$  is the electron current at the anode-organic contact, which forms a high leakage current. (b) The complete  $J-V$  curves calculated under the same conditions as those of (a). The disorder parameter  $\sigma$  is set to 80 meV in all of the calculations.

of the total photocurrent reverse quickly and leading to an anomalous reduction of the  $V_{\text{oc}}$ . The same situation also applies to the hole current extracted from the cathode, which contributes to the other component of the large leakage current. This kind of  $V_{\text{oc}}$  loss arises purely from a disorder-induced mobility reduction which subsequently changes charge dynamics under steady state, and thus it displays different behavior than that due to the charge filling in disordered energy levels.

Now, it is understandable why the  $V_{\text{oc}}$  does not decrease when the Onsager-Braun theory is assumed in the device model because, in this case, the reduction of free charge carriers with the decreasing temperature is so quick that there are very few carriers being extracted from the wrong electrode and the undesirable leakage current is negligible. With charge-extraction efficiency being improved by employing materials of high mobilities, the photocurrent may overcome the leakage current and circumvent the drastic reduction of the  $V_{\text{oc}}$  to some extent, as is shown in Fig. 5(a). The leakage current can be more effectively quenched by inserting blocking layers between the electrode and the active layer, but the reduction of photocurrent remains unavoidable at low temperatures.

#### IV. CONCLUSIONS

In this work, we employ a one-dimensional device-model simulation method to investigate the anomalous reduction of the open-circuit voltage at low temperatures in organic solar cells. The  $V_{\text{oc}} - T$  plots are calculated under varied charge generation rates, charge-carrier mobilities, metal-organic contact types, and many other different conditions. It is found that, with a strongly temperature-dependent Onsager-Braun-type charge generation rate, the  $V_{\text{oc}}$  simply follows the common behavior of linear increases as the temperature decreases and, finally, saturates, which implies that the reduced charge-carrier density at low temperatures is not sufficient for explaining the anomalous reduction behavior. For nonselective contacts, when incorporating the energetic disorder-suppressed mobilities but keeping the charge generation rate constant or slowly varying with the decreasing

temperature, the reduction behavior of the  $V_{\text{oc}}$  indeed emerges at low temperatures. The larger the disorder parameter, the higher the critical temperature below which the  $V_{\text{oc}}$  begins to decrease. The critical temperature declines if the charge extraction efficiency is improved by enhancing the high- $T$  limit of mobilities or reducing the thickness of the active layer. On the other hand, for selective contacts, the  $V_{\text{oc}}$  does not decrease at low temperatures—no matter how large  $\sigma$  is. The ultrahigh  $V_{\text{oc}}$  loss effect reveals that, at low temperatures, with the decreased BR rate and the low interfacial majority-carrier density, free charge carriers are mostly lost through extraction by the respective wrong electrodes rather than the internal recombination, leading to a high leakage current. The leakage current counteracts the current for majority-carrier extraction until the total photocurrent vanishes at small voltage, which causes the reduced open-circuit voltages. Further works on the  $V_{\text{oc}}$  loss mechanism can be done through investigating the charge-carrier loss pathways in their steady-state dynamics.

#### ACKNOWLEDGMENTS

The authors acknowledge financial support from the National Natural Science Foundation of China under Grants No. 11604280, No. 61574122, No. 51602276, No. 91333202, and No. 11574052. W. Y. is also supported by the Nanhu research program for young investigators of Xinyang Normal University.

- [1] C. Deibel and D. Dyakonov, Polymer-fullerene bulk heterojunction solar cells, *Rep. Prog. Phys.* **73**, 096401 (2010).
- [2] J. Yao, T. Kirchartz, M. S. Vezie, M. A. Faist, W. Gong Z. He, H. Wu, J. Troughton, T. Watson, D. Bryant, and J. Nelson, Quantifying Losses in Open-Circuit Voltage in Solution-Processable Solar Cells, *Phys. Rev. Applied* **4**, 014020 (2015).
- [3] C. Deibel, T. Strobel, and V. Dyakonov, Role of the charge transfer state in organic donor/acceptor solar cells, *Adv. Mater.* **22**, 4097 (2010).

- [4] K. Vandewal, K. Tvingstedt, A. Gadisa, O. Inganäs, and J. V. Manca, On the origin of the open-circuit voltage of polymer-fullerene solar cells, *Nat. Mater.* **8**, 904 (2009).
- [5] K. Vandewal, K. Tvingstedt, A. Gadisa, O. Inganäs, and J. V. Manca, Relating the open-circuit voltage to interface molecular properties of donor:acceptor bulk heterojunction solar cells, *Phys. Rev. B* **81**, 125204 (2010).
- [6] T. M. Burke, S. Sweetnam, K. Vandewal, and M. D. McGehee, Beyond Langevin recombination: How equilibrium between free carriers and charge transfer states determines the open-circuit voltage of organic solar cells, *Adv. Energy Mater.* **5**, 1500123 (2015).
- [7] Y. Zou and R. J. Holmes, Correlation between the open-circuit voltage and charge transfer state energy in organic photovoltaic cells, *ACS Appl. Mater. Interfaces* **7**, 18306 (2015).
- [8] Z. Guan, H.-W. Li, Y. Cheng, Q. Yang, M.-F. Lo, T.-W. Ng, S.-W. Tsang, and C.-S. Lee, Charge-transfer state energy and its relationship with open-circuit voltage in an organic photovoltaic device, *J. Phys. Chem. C* **120**, 14059 (2016).
- [9] A. Maurano, R. Hamilton, C. G. Shuttle, A. M. Ballantyne, J. Nelson, B. O'Regan, W. Zhang, I. McCulloch, H. Azimi, M. Morana, C. J. Brabec, and J. R. Durrant, Recombination dynamics as a key determinant of open circuit voltage in organic bulk heterojunction solar cells: A comparison of four different donor polymers, *Adv. Mater.* **22**, 4987 (2010).
- [10] O. J. Sandberg, A. Sundqvist, M. Nyman, and R. Österbacka, Relating Charge Transport, Contact Properties, and Recombination to Open-Circuit Voltage in Sandwich-Type Thin-Film Solar Cells, *Phys. Rev. Applied* **5**, 044005 (2016).
- [11] D. Rauh, A. Wagenpfahl, C. Deibel, and V. Dyakonov, Relation of open circuit voltage to charge carrier density in organic bulk heterojunction solar cells, *Appl. Phys. Lett.* **98**, 133301 (2011).
- [12] J. C. Blakesley and D. Neher, Relationship between energetic disorder and open-circuit voltage in bulk heterojunction organic solar cells, *Phys. Rev. B* **84**, 075210 (2011).
- [13] G. Garcia-Belmonte, Temperature dependence of open-circuit voltage in organic solar cells from generation-recombination kinetic balance, *Sol. Energy Mater. Sol. Cells* **94**, 2166 (2010).
- [14] G. Garcia-Belmonte and J. Bisquert, Open-circuit voltage limit caused by recombination through tail states in bulk heterojunction polymer-fullerene solar cells, *Appl. Phys. Lett.* **96**, 113301 (2010).
- [15] S. D. Collins, C. M. Proctor, N. A. Ran, and T.-Q. Nguyen, Understanding open-circuit voltage loss through the density of states in organic bulk heterojunction solar cells, *Adv. Energy Mater.* **6**, 1501721 (2016).
- [16] L. J. A. Koster, V. D. Mihailetschi, R. Ramaker, and P. W. M. Blom, Light intensity dependence of open-circuit voltage of polymer:fullerene solar cells, *Appl. Phys. Lett.* **86**, 123509 (2005).
- [17] V. V. Brus, Light dependent open-circuit voltage of organic bulk heterojunction solar cells in the presence of surface recombination, *Org. Electron.* **29**, 1 (2016).
- [18] M. D. Perez, C. Borek, S. R. Forrest, and M. E. Thompson, Molecular and morphological influences on the open circuit voltages of organic photovoltaic devices, *J. Am. Chem. Soc.* **131**, 9281 (2009).
- [19] O. J. Sandberg, M. Nyman, and R. Österbacka, Effect of Contacts in Organic Bulk Heterojunction Solar Cells, *Phys. Rev. Applied* **1**, 024003 (2014).
- [20] V. D. Mihailetschi, L. J. A. Koster, and P. W. M. Blom, Effect of metal electrodes on the performance of polymer:fullerene bulk heterojunction solar cells, *Appl. Phys. Lett.* **85**, 970 (2004).
- [21] W. Yang, Y. Yao, and C. Q. Wu, Mechanisms of device degradation in organic solar cells: Influence of charge injection at the metal/organic contacts, *Org. Electron.* **14**, 1992 (2013).
- [22] N. K. Elumalai and A. Uddin, Open circuit voltage of organic solar cells: An in-depth review, *Energy Environ. Sci.* **9**, 391 (2016).
- [23] U. Rau, Reciprocity relation between photovoltaic quantum efficiency and electroluminescent emission of solar cells, *Phys. Rev. B* **76**, 085303 (2007).
- [24] B. P. Rand, D. P. Burk, and S. R. Forrest, Offset energies at organic semiconductor heterojunctions and their influence on the open-circuit voltage of thin-film solar cells, *Phys. Rev. B* **75**, 115327 (2007).
- [25] U. Hörmann, J. Kraus, M. Gruber, C. Schuhmair, T. Linderl, S. Grob, S. Kapfinger, K. Klein, M. Stutzman, H. J. Krenner, and Wolfgang Brütting, Quantification of energy losses in organic solar cells from temperature-dependent device characteristics, *Phys. Rev. B* **88**, 235307 (2013).
- [26] G. Grancini, M. Maiuri, D. Fazzi, A. Petrozza, H.-J. Egelhaaf, D. Brida, G. Cerullo, and G. Lanzani, Hot exciton dissociation in polymer solar cells, *Nat. Mater.* **12**, 29 (2013).
- [27] X. Zhu, N. R. Monahan, Z. Gong, H. Zhu, K. W. Williams, and Cory A. Nelson, Charge transfer excitons at van der Waals interfaces, *J. Am. Chem. Soc.* **137**, 8313 (2015).
- [28] Y. Liu, K. Zojer, B. Lassen, J. K. -Hansen, H.-G. Rubahn, and M. Madsen, Role of the charge-transfer state in reduced Langevin recombination in organic solar cells: A theoretical study, *J. Phys. Chem. C* **119**, 26588 (2015).
- [29] F. Gao, W. Tress, J. Wang, and O. Inganäs, Temperature Dependence of Charge Carrier Generation in Organic Photovoltaics, *Phys. Rev. Lett.* **114**, 128701 (2015).
- [30] B. A. Gregg, Entropy of charge separation in organic photovoltaic cells: The benefit of higher dimensionality, *J. Phys. Chem. Lett.* **2**, 3013 (2011).
- [31] N. R. Monahan, K. W. Williams, B. Kumar, C. Nuckolls, and X.-Y. Zhu, Direct Observation of Entropy-Driven Electron-Hole Pair Separation at an Organic Semiconductor Interface, *Phys. Rev. Lett.* **114**, 247003 (2015).
- [32] P. S. Davids, I. H. Campbell, and D. L. Smith, Device model for single carrier organic diodes, *J. Appl. Phys.* **82**, 6319 (1997).
- [33] L. J. A. Koster, E. C. P. Smits, V. D. Mihailetschi, and P. W. M. Blom, Device model for the operation of polymer/fullerene bulk heterojunction solar cells, *Phys. Rev. B* **72**, 085205 (2005).
- [34] B. Y. Finck and B. J. Schwartz, Drift-Diffusion Modeling of the Effects of Structural Disorder and Carrier Mobility on the Performance of Organic Photovoltaic Devices, *Phys. Rev. Applied* **4**, 034006 (2015).
- [35] T. M. Clarke and J. R. Durrant, Charge photogeneration in organic solar cells, *Chem. Rev.* **110**, 6736 (2010).

- [36] C. Deibel, A. Wagenpfahl, and V. Dyakonov, Origin of reduced polaron recombination in organic semiconductor devices, *Phys. Rev. B* **80**, 075203 (2009).
- [37] M. C. Heiber, C. Baumbach, V. Dyakonov, and C. Deibel, Encounter-Limited Charge-Carrier Recombination in Phase-Separated Organic Semiconductor Blends, *Phys. Rev. Lett.* **114**, 136602 (2015).
- [38] G. Lakhwani, A. Rao, and R. H. Friend, Bimolecular recombination in organic photovoltaics, *Annu. Rev. Phys. Chem.* **65**, 557 (2014).
- [39] H. Bässler, Charge photogeneration in organic solar cells, *Phys. Status Solidi B* **175**, 15 (1993).
- [40] S. D. Baranovskii, H. Cordes, F. Hensel, and G. Leising, Charge-carrier transport in disordered organic solids, *Phys. Rev. B* **62**, 7934 (2000).
- [41] W. F. Pasveer, J. Cottaar, C. Tanase, R. Coehoorn, P. A. Bobbert, P. W. M. Blom, D. M. de Leeuw, and M. A. J. Michels, Unified Description of Charge-Carrier Mobilities in Disordered Semiconducting Polymers, *Phys. Rev. Lett.* **94**, 206601 (2005).
- [42] V. Coropceanu, J. Cornil, D. A. da Silva Filho, Y. Olivier, R. Silbey, and J.-L. Brédas, Charge transport in organic semiconductors, *Chem. Rev.* **107**, 926 (2007).
- [43] M. Kuik, G.-J. A. H. Wetzelaer, H. T. Nicolai, N. I. Craciun, D. M. De Leeuw, and P. W. M. Blom, Charge transport and recombination in polymer light-emitting diodes, *Adv. Mater.* **26**, 512 (2014).
- [44] A. A. Bakulin, A. Rao, V. G. Pavelyev, P. H. M. van Loosdrecht, M. S. Pshenichnikov, D. Niedzialek, J. Cornil, D. Beljonne, and R. H. Friend, The role of driving energy and delocalized states for charge separation in organic semiconductors, *Science* **335**, 1340 (2012).
- [45] L. G. Kaake, D. Moses, and A. J. Heeger, Coherence and uncertainty in nanostructured organic photovoltaics, *J. Phys. Chem. Lett.* **4**, 2264 (2013).
- [46] K. B. Whaley, A. A. Kocherzhenko, and A. Nitzan, Coherent and diffusive time scales for exciton dissociation in bulk heterojunction photovoltaic cells, *J. Phys. Chem. C* **118**, 27235 (2014).
- [47] A. Foertig, A. Baumann, D. Rauh, V. Dyakonov, and C. Deibel, Charge carrier concentration and temperature dependent recombination in polymer-fullerene solar cells, *Appl. Phys. Lett.* **95**, 052104 (2009).
- [48] A. J. Barker, K. Chen, and J. M. Hodgkiss, Distance distributions of photogenerated charge pairs in organic photovoltaic cells, *J. Am. Chem. Soc.* **136**, 12018 (2014).